Cyclin N-terminal domain-containing 1 (CNTD1) is critical for crossover designation during meiotic prophase I and for maintenance of ovarian reserve in mammalian oocytes

Anna Wood, Rania M. Ahmed, Rachel A. Bradley, Ian D. Wolff, and Paula E. Cohen*

Affiliation: Department of Biomedical Sciences and Cornell Reproductive Sciences Center (CoRe), Cornell University, Ithaca, NY 14853, USA

*Correspondence:

KEYWORDS: meiosis, crossing over, CNTD1, female, oocyte, prophase I, mouse

Corresponding author: Paula E. Cohen (paula.cohen@cornell.edu)

ABSTRACT

In meiotic prophase I, hundreds of double-strand breaks (DSB) are induced to initiate homologous recombination, resulting in the formation of non-crossovers (NCO) and crossovers (CO). Of the 250-300 DSBs that form in mice, only ~10% are resolved as COs, with all remaining DSB events resolving as NCO. Thus, both the frequency and distribution of COs must be tightly regulated to ensure their appropriate localization across the genome. Errors in crossover designation and maturation can result in nondisjunction, leading to aneuploidy, germ cell death, birth defects, or infertility. That these errors are more evident in female meiosis compared to males suggests that the events of meiotic prophase I are sexually dimorphic with respect to DSB processing, resolution, and/or surveillance. Therefore, it is essential to investigate how COs are designated and regulated during prophase I in the female germline. Previous studies in our lab showed that Cyclin N-Terminal Domain Containing 1 (CNTD1) protein plays a critical role in CO designation during male meiosis, co-localizing with other essential CO proteins such as MutLγ (MLH1/MLH3) and crossover site-associated cyclin-dependent kinase-2 (CDK2) during pachynema. In the current study, we investigated whether analogous roles for CNTD1 existed in female meiosis. Similar to *Cntd1*$^{-/-}$ males, *Cntd1*$^{-/-}$ females are sterile, with no gross morphological ovarian defects in adults albeit with a depletion in ovarian follicle numbers. During prophase I, early DSB induction and repair occur normally, but oocytes from *Cntd1*$^{-/-}$ females fail to accumulate MutLγ in pachynema. Phenotypically, meiotic prophase I disruption in *Cntd1*$^{-/-}$ females is similar to that seen in *Cntd1*$^{-/-}$ males. Importantly, whereas the *Caernohabditis elegans* ortholog of CNTD1, COSA-1, appears to interact with CDK-2 during pachynema in oocytes, CNTD1 in mouse oocytes lacks the CDK-interacting motif, suggesting that its function in oocytes does not involve a cyclin-like induction of CDK2 phosphorylation activity. In contradiction to the timing of prophase I disruption in *Cntd1*$^{-/-}$ females at pachynema, we observe a dramatic depletion of primordial follicles, beginning shortly after birth and increasing dramatically through to adult ages. Those primordial follicles that persist, however, are able to develop through dictyate arrest into primary and larger follicular structures in pre-pubertal females, and only by adulthood were significant declines observed in all follicles. The early loss of oocytes in *Cntd1*$^{-/-}$ females shortly after birth, considerably earlier than that observed for mice lacking MLH1 or MLH3, suggests a novel early role for CNTD1 in CO designation and/or in ensuring progression of oocytes into dictyate arrest at late pachynema.

INTRODUCTION

Meiosis is a unique cellular division that gives rise to haploid gametes for sexual reproduction. In contrast to mitosis, meiosis consists of two chromosome divisions preceeded by only a single round of DNA replication. During meiosis I, homologous parental chromosomes must find each other, pair and then segregate equally at the first meiotic division, resulting in up to two daughter cells that then enter meiosis II. The second division is reminiscent of mitosis in that it involves the segregation of sister chromatids that are already paired through the network of cohesion complexes that ensure their persistent connection. Thus, the faithful pairing and segregation of homologous chromosomes during meiosis I is particularly critical to ensure euploid gametes, and is dependent on the hundreds of DNA double strand breaks (DSB) that are formed at the start of prophase I, each of which must be repaired with absolute fidelity prior to metaphase I entry. The majority of DSBs (~90%) are repaired as non-crossovers (NCO) which do not involve exchange of flanking DNA sequence between homologous chromosomes. Remarkably, only a small subset (10%) of these DSBs will be repaired as crossovers (CO) that are crucial for ensuring the persistence of homolog interactions until the first meiotic division. Given the importance of COs in ensuring persistent homolog interactions, therefore, it is not surprising that the distribution and frequency of COs across the genome must be tightly regulated to prevent chromosome non-disjunction. However, there appears to be distinct sexual dimorphism in the success of these events in mammalian meiosis, as underscored by the fact that that nearly 70% of human oocytes exhibit aneuploidy in comparison to only 3-5% of spermatocytes (Wang et al. 2017; Hassold and Hunt 2001; Nagaoka et al. 2012; Hunt and Hassold 2008; Gruhn et al. 2013; Morelli and Cohen 2005; Gruhn and Hoffmann 2022). Interestingly, but somewhat unsurprisingly, a majority of nondisjunction events occur at the first meiotic division, arising from defects in crossover placement and designation. This raises the question of how CO regulation may differ between the sexes in mammals.

The majority of our knowledge of DSB repair and CO formation in mammalian meiosis comes from studies in male mice. In males, meiotic recombination involves a series of tightly regulated events downstream of DSB induction that begins with processing of DSBs to create single-stranded overhangs capable of invading an opposing homolog to test for homology. The initiation of DSBs is catalyzed by the topoisomerase-like protein SPO11 and its crucial partner proteins (Keeney et al. 1997; Romanienko and Camerini-Otero 2000; Gray and Cohen 2016; Tran

and Schimenti 2019). Subsequently, the RecA homologs RAD51 and DMC1 facilitate the induction of homology search for either the repair of these DSBs between sister chromatids or homologous chromosomes (Cao et al., 1990; Cloud et al., 2012). The latter are further processed into COs by a highly regulated network of pro-CO proteins.

The DNA mismatch repair MutS homologs, MSH4 (MutS Homolog 4) and MSH5 (MutS Homolog 5), which form a heterodimer known as MutSγ, associate with a subset of DSB repair intermediates in a process termed CO licensing (de Vries et al., 1999; Edelmann et al., 1999; Gray and Cohen, 2016; Kneitz et al., 2000). Licensing also appears to require recruitment of RNF212 (Ring Finger protein 12). Importantly, however, not all MutSγ/RNF212-loaded sites are destined to become COs in mammals. Instead, the final designation of COs requires the recruitment of a group of regulators including HEI10 (Human Enhancer of Invasion 10), CNTD1 (Cyclin N-terminal domain containing-1 protein), PRR19 (Proline-rich protein 19), and CDK2 (Cyclin-dependent kinase 2) (Bondarieva et al., 2020; Gray et al., 2020; Holloway et al., 2014; Palmer et al., 2020; Qiao et al., 2014; Reynolds et al., 2013; Ward et al., 2007), along with a heterodimer of the MutL homologs, MLH1 (MutL Homolog 1) and MLH3 (MutL Homolog 3), collectively named MutLγ. Together, these proteins mark the final subset of DSBs that will become COs of the major class I category (Edelmann et al., 1996; Kolas et al., 2005; Lipkin et al., 2002; Toledo et al., 2019; Woods et al., 1999). In mouse, class I COs represent 90-95% of all COs, and these accumulate across the genome at a frequency of 22-24 in males and 24-26 in females (Gray and Cohen, 2016; Lenzi et al., 2005). How a subset of the ~150 MutSγ sites are designated to become COs is a major question in the field.

Previous studies in our lab revealed a critical role for CNTD1 in the process of crossover designation in male meiosis. CNTD1 was identified as an ortholog of the *C. elegans* Crossover Site-Associated-1 (COSA-1) (Yokoo et al., 2012). *cosa-1* mutants exhibit a high rate of inviable embryos and a significant increase in autosomal mis-segregation due to an absence of chiasmata, establishing *cosa-1* as a pro-CO factor (Yokoo et al. 2012). Interestingly, COSA-1 is a cyclin B-related protein, and recent studies have demonstrated that COSA-1 interacts physically with the cyclin-dependent kinase, CDK-2, to phosphorylate the C-terminus of MSH-5 to stabilize its association at sites of crossovers (Haversat et al., 2022).

In mice, CNTD1 appears at pachynema of prophase I where it co-localizes with MutLγ and CDK2 (Gray et al., 2020; Holloway et al., 2014). Loss of CNTD1 in *Cntd1*$^{-/-}$ males results in the

complete absence of epididymal spermatozoa leading to infertility (Gray et al., 2020; Holloway et
120 al., 2014). During prophase I, spermatocytes from *Cntd1*$^{-/-}$ males show normal progression through leptonema and zygonema, including normal assembly of the synaptonemal complex and early DSB processing stages. By pachynema, however, spermatocytes from *Cntd1*$^{-/-}$ males fail to undergo normal CO designation, characterized by persistently elevated MutSγ focus frequency through to late pachynema, and failure to accumulate CO-associated MutLγ and CDK2 (Gray et al., 2020;
125 Holloway et al., 2014). Interestingly, and unlike the situation for worm COSA-1, CNTD1 in the male mouse lacks a critical cyclin homology domain predicted to be within the full-length genomic sequence, possibly through transcription of a truncated mRNA (Gray et al., 2020). As a result, both yeast two-hybrid analysis and immunoprecipitation from testis extracts reveals that the testis CNTD1 is incapable of binding to CDK2 and thus does not act as a canonical cyclin during
130 prophase I in the mouse, suggesting a different mechanism of action to that of COSA-1 (Gray et al., 2020; Haversat et al., 2022; Yokoo et al., 2012).

Given the sexual dimorphism in prophase I regulation observed in mammals, we were interested in investigating the role of CNTD1 in female meiosis. In contrast to the meiotic program in males, which initiates at sexual maturity and progresses continuously throughout life, meiosis
135 in mammalian females begins during fetal development. More specifically, only the first meiotic prophase I is completed in oocytes then meiosis halts, resulting in a unique stage called dictyate arrest. It is not until sexual maturity when meiosis I resumes only for a small cohort of oocytes. These select oocytes are arrested again at the end of metaphase II, and only at fertilization does the meiotic program complete (Morelli and Cohen, 2005). We find that *Cntd1* homozygous mutant
140 females are sterile due to a dramatic decrease in primordial follicles before sexual maturity along with an almost complete failure to form chiasmata due to the loss of crossover-associated CDK2 and MutLγ. Interestingly, we also find CNTD1 acts in a cyclin-independent mechanism, previously reported for male meiosis, implying its molecular function in CO designation is the same in oocytes and spermatocytes.

145

RESULTS

Oocytes from *Cntd1*$^{-/-}$ female mice show a complete absence of class I crossovers.

To determine the localization of CNTD1 in oocytes, we generated chromosome spreads
150 from ovaries of mouse embryos at 18.5 days post-coitum (dpc) which corresponds to the developmental time point during which most of the germ cells are in pachynema of prophase I (Hwang et al., 2018; Sun and Cohen, 2013). We utilized two lines of mice, generated in our previous studies (Gray et al., 2020): the first bearing a null allele of *Cntd1*, referred to as *Cntd1*$^{-/-}$, and the second harboring a tandem FLAG and HA-tagged variant of *Cntd1*, referred to as
155 *Cntd1*$^{HA/HA}$. The *Cntd1*^{HA} allele behaves much like the wildtype allele, and thus, for all our experiments, we maintained both alleles within the same mouse colony, using *Cntd1*$^{HA/HA}$ mice as our wildtype controls, *Cntd1*$^{HA/-}$ mice as our heterozygous animals, and *Cntd1*$^{-/-}$ mice as our homozygous mutant test mice. Following chromosome spreading, oocyte nuclei were stained with antibodies against a component of the axial element, SYCP3 (Synaptonemal Complex Protein 3)
160 and either the HA epitope for CNTD1 visualization (Fig. 1A) or MLH1 for class I CO maturation (Fig. 1E). We also performed co-localizaton of CNTD1 and MLH1 by combining both antibodies (Suppl. Fig. 1). CNTD1 was detected as discrete foci localized to the synaptonemal complex in pachytene-staged oocytes in a pattern and frequency reminiscent of the terminal crossover factors, MLH1 and MLH3 (Fig. 1A,B,D). CNTD1^{HA} was observed at a frequency of 27.35 foci on spreads
165 from *Cntd1*$^{HA/HA}$ females and 25.67 foci on spreads from *Cntd1*$^{HA/-}$ females (Fig. 1D). As expected, *Cntd1*$^{-/-}$ oocytes did not show the presence of CNTD1^{HA} on chromosome spreads (Fig. 1C). This is consistent with our published work characterizing the function of CNTD1 in mammalian spermatogenesis (Gray et al., 2020).

To explore the distribution of class I crossover events across the genome in the absence of
170 CNTD1, chromosome spreads were prepared from mice of all genotypes, and stained with antibodies against SYCP3 and MLH1. We observed MLH1 at an average frequency of 26.75 and 25.46 foci in *Cntd1*$^{HA/HA}$ and *Cntd1*$^{HA/-}$ oocyctes, respectively (Fig. 1E,F,H). *Cntd1*$^{-/-}$ oocytes exhibited a complete loss of MLH1 on the synaptonemal complex in pachynema (Fig. 1G). Similar to our findings in *Cntd1*$^{-/-}$ males, the absence of MLH1 indicates that CNTD1 is either acting
175 upstream of MutLγ, or that CNTD1 is necessary for MutLγ accumulation at sites of COs.

To investigate co-localization of CNTD1 and MutLγ, we used antibodies against HA in conjunction with our custom-made antibodies against MLH3 (Gray et al. 2020). On average, 89.25% and 93.44% of CNTD1 foci were found to co-localize with MLH3 at pachynema in spreads from Cntd1$^{HA/HA}$ and *Cntd1*$^{HA/-}$ oocytes, respectively. Conversely, 91.53% and 87.34% of

180 MLH3 foci localized with CNTD1 in *Cntd1*$^{HA/HA}$ and *Cntd1*$^{HA/-}$ oocytes, respectively (Suppl. Fig 1). The close co-localization pattern of CNTD1 with MLH3 lends evidence to the function of the former as a class I crossover regulator. This result is also supported by the equivalent number of MLH1 and CNTD1 foci at pachytene (Fig 1D, H). Although the colocalization pattern is not absolute, this discrepancy can be explained by the relative difficulty of sub-staging pachytene-
185 staged oocytes.

Crossover maturation is disrupted in *Cntd1*$^{-/-}$ females.

At the end of prophase I, COs manifest into physical linkages holding homologous chromosomes together, known as chiasmata. We found that chiasmata formation was normal in
190 *Cntd1*$^{HA/HA}$ and *Cntd1*$^{HA/-}$ oocytes, with 26.35 and 25.09 chiasmata per cell, respectively (red arrows, Fig. 1I, J, and L). However, *Cntd1*$^{-/-}$ oocytes showed a significant decline in chiasmata formation resulting in an increase of univalent chromosomes (blue arrow, Fig. 1K). However, *Cntd1*$^{-/-}$ oocytes retained on average 1.16 chiasmata per cell (Fig. 1L), reflecting an approximately 95% loss of COs, presumably indicative of a functional class II crossover pathway, albeit at a
195 slightly reduce rate of use to that seen in male meiosis (Holloway et al., 2014, 2008). Taken together, these results indicate that *Cntd1* is essential for class I crossover formation, which is consistent with the model that CNTD1 is involved in regulating MLH1 placement, but not essential for class II crossover formation due to persistence of a small number of residual chiasmata.

200 **CNTD1 is expressed in a truncated isoform lacking critical cyclin homology domains.**

Like its nematode ortholog, COSA-1, full-length CNTD1 is predicted to act as a cyclin due to the presence of three cyclin homology regions at amino acid positions 57-88, 117-135, and 140-180 (Gray et al. 2020). However, *in silico* analysis of the *Cntd1* coding sequence shows a highly conserved second methionine at amino acid position 86 (in mouse), which results in a truncation
205 of the predicted full-length protein to produce a short-form CNTD1 (CNTD1^{SF}) protein of 249 amino acids in length (compared to the 334 amino acid length of the full-length protein). CNTD1^{SF} lacks the ability to interact with crossover associated CDK2, its putative kinase interactor, in both yeast two-hybrid assays and co-immunoprecipitations which is consistent with other reports (Bondarieva et al., 2020; Gray et al., 2020). Importantly, CNTD1^{SF} is the only form of CNTD1
210 found in mouse spermatocytes, or indeed in any tissue in male mice (Gray et al., 2020). Therefore,

we were curious to know if CNTD1 existed in the same short form in mouse oocytes, or perhaps the use of an alternative isoform of CNTD1 in female mice could provide an explanation for the sexual dimorphism in prophase I outcomes between males and females.

We performed a co-immunoprecipitation (co-IP) with antibodies against HA to isolate CNTD1-HA from lysate generated from fetal ovaries collected at 18.5 dpc, a timepoint corresponding to pachynema, and then probed via western blot (WB) with anti-HA antibody to determine which isoform of CNTD1 was expressed in oocytes. CNTD1-HA was present at the same predicted molecular weight (~29.7 kDa) in oocytes (*Cntd1*$^{HA/HA}$ ♀) as in spermatocytes (*Cntd1*$^{HA/HA}$ ♂) (Fig. 2A). As expected, we did not find HA-tagged CNTD1 in fetal whole ovary lysate from C57BL/6J females (C57BL/6J ♀). Taken together, this data supports our previous study showing CNTD1 exists *in vivo* in an isoform lacking the first cyclin homology domain, and suggests that CNTD1 is functioning via a cyclin independent mechanism in mammalian oocytes.

Absence of *Cntd1* results in sterility and loss of primordial follicles.

Disruption of crossover designation factors results in complete sterility and manifests in a phenotype characterized by gross morphological defects in gonadal tissues, including a significant decrease in testis size coupled with a significant loss of meiocytes and loss of post meiotic cells in testis tissue sections (Bondarieva et al., 2020; Gray et al., 2020; Holloway et al., 2014). Morphological effects appear to be bifurcated in females where there are two distinct phenotypes. The first is observed in mutants that affect early DSB repair events, and leads to a significant reduction in ovarian size and lack of folliculogenesis resulting from disruption of meiotic prophase prior to pachynema. This phenotypic category is represented by mouse mutants lacking genes such as *Dmc1, Msh4, and Msh5* (Edelmann et al., 1999; Kneitz et al., 2000; Pittman et al., 1998; Yoshida et al., 1998). The second phenotypic category is characterized by later prophase I disruption from pachynema onwards, resulting in normal ovarian morphology and follicle composition. Oocytes from these mutant mice can complete the first meiotic division post-natally, but show severe non-disjunction at the first meiotic division, and subsequent failure to produce viable embryos. Gene mutations in this second category include *Mlh1*, and *Mlh3* (Edelmann et al., 1996; Lipkin et al., 2002). Reports from studies of genes involved in CO licensing and/or designation, including *Rnf212*, *Hei10*, and *Prr19*, suggest a similar ovarian phenotype to that described for the second phenotypic category—similar to phenotypes of MutLγ-deficient mice—

but have yet to be fully characterized (Bondarieva et al., 2020; Qiao et al., 2014; Reynolds et al., 2013; Ward et al., 2007). Due to the temporal accumulation of CNTD1, and its co-localization with HEI10 and PRR19 (Bondarieva et al., 2020), we hypothesized a similar temporal phenotype for *Cntd1* females, namely no loss of follicle structures or ovarian morphology in adult mice, but producing oocytes that are incapable of completing a normal first meiotic division.

To explore the consequences of CNTD1 dysfunction in the oocyte for ovarian development and folliculogenesis, we investigated fertility, ovarian morphology, and follicle populations using *Cntd1*$^{HA/HA}$ animals as our wildtype control cohort together with *Cntd1*$^{HA/-}$ and *Cntd1*$^{-/-}$ females. *Cntd1*$^{-/-}$ females were unable to produce litters after approximately three months housed with a *Cntd1*$^{HA/HA}$ male (Supplementary Figure 2), confirming that these animals are infertile. To determine if ovaries from *Cntd1*$^{-/-}$ females exhibit early or late prophase I disruption, we quantitated the ovarian follicular composition from pre-pubertal post-natal day 1 (PND 1), post-natal day 14 (PND 14), post-natal day 28 (PND 28), and adult (8-12 week old) females (n≥3 for each time point), documenting the follicular stages from primordial (early) follicles through antral (late pre-ovulatory) follicles.

The average population of primordial follicles was significantly decreased in *Cntd1*$^{-/-}$ females compared to *Cntd1*$^{HA/HA}$ littermate controls at PND 14 (*Cntd1*$^{HA/HA}$ n=1595; *Cntd1*$^{HA/-}$ n=1249; and *Cntd1*$^{-/-}$ n=258), PND 28 (*Cntd1*$^{HA/HA}$ n=1250; *Cntd1*$^{HA/-}$ n=935; and *Cntd1*$^{-/-}$ n=100), and adult (*Cntd1*$^{HA/HA}$ n=478; *Cntd1*$^{HA/-}$ n=374; and *Cntd1*$^{-/-}$ n=125) timepoints (Fig. 3E-H, I-L, and M-P). At PND1, although combined germ cell cyst and primordial follicle numbers were reduced to approximately 48% of that in *Cntd1*$^{HA/HA}$ littermate control ovaries, (*Cntd1*$^{HA/HA}$ n=460; *Cntd1*$^{HA/-}$ n=423; and *Cntd1*$^{-/-}$ n=238) this decline was not significant (p=0.1112, Fig. 3A-D), likely due to the high variability in counting at this age since many oocytes may have already undergone programmed apoptosis (atresia) at this stage, with others soon to become atretic. The first stage of follicular growth is represented by the appearance of primary staged follicles, which are apparent at the PND14 timepoint onwards, and these exhibited a significant decrease in *Cntd1*$^{-/-}$ females compared to *Cntd1*$^{HA/HA}$ littermate controls at PND28 (*Cntd1*$^{HA/HA}$ n=241; *Cntd1*$^{HA/-}$ n=200; and *Cntd1*$^{-/-}$ n=86) and adulthood (*Cntd1*$^{HA/HA}$, n=236, *Cntd1*$^{HA/-}$, n=240, and *Cntd1*$^{-/-}$, n=26) (Fig. 3L, P). Secondary and antral follicles were not different between genotypes at PND14 and PND28, but all stages of follicles at the adult timepoint showed a significant decrease in *Cntd1*$^{-/-}$ ovaries compared to that of *Cntd1*$^{HA/HA}$ females (Fig. 3P). This suggests that the few primordial

follicles that are able to progress through folliculogenesis can then undergo normal development, however the oocytes are inviable. The loss of primordial follicles in the absence of CNTD1 only
275 starts to impact primary, secondary and antral follicles from PND 28 onwards. Together, these data indicate that oocytes from *Cntd1*$^{-/-}$ mice start to undergo apoptosis from birth and before follicle formation occurs, at some point between the end of prophase I and before PND 14, and that this continues in a dramatic fashion as the mice progress towards adulthood. This pattern of early primordial follicle loss is unexpected given the temporal accumulation of CNTD1 at sites of
280 crossovers in pachynema and the late appearance of prophase I defects in *Cntd1*$^{-/-}$ mice, which show normal progression into pachynema.

Synapsis and DSB formation are normal in *Cntd1*$^{-/-}$ oocytes and do not contribute to loss of primordial follicles.

285 Incomplete synapsis of homologous chromosomes and unrepaired DSBs during meiotic prophase I in oocytes can trigger synapsis and DSB checkpoints (e.g., Dual-Checkpoint Model), which can lead to apoptosis in the absence of repair (Bolcun-Filas et al., 2014; Ravindranathan et al., 2022; Rinaldi et al., 2020, 2017). To assess if early DSB repair and recombination events are affected in *Cntd1*$^{-/-}$ oocytes, we used an antibody against the RecA homolog, RAD51 to stain
290 spread chromosomes in leptotene through diplotene-staged oocytes in all *Cntd1* genotypes (Fig. 4A-L). All genotypes showed canonical staining patterns in which RAD51 accumulated as expected in zygotene-staged oocytes (Fig. 4D-F) and was almost completely absent by pachynema (Fig. 4G-I), indicating normal progression of DSB repair past the strand invasion stages. Upon analysis of RAD51 foci at pachynema, however, *Cntd1*$^{HA/HA}$ (average n=3.82 foci) and *Cntd1*$^{HA/-}$
295 (average n=2.86 foci) showed a modest, but not significant difference in RAD51 foci in comparison to *Cntd1*$^{-/-}$ (average n=4.97 foci) oocytes (Fig. 4M). Given that it is very difficult to classify sub-stages of pachynema in oocytes, it is likely that any early pachytene persistence of RAD51 observed in the oocytes from *Cntd1*$^{-/-}$ ovaries is masked by the later recovery of the RAD51 profile in later pachytene stages. These data indicate that early DSB repair events proceed
300 normally in the absence of CNTD1 albeit with perhaps a slight delay in removal of RAD51 in early pachynema.

Previous work from our lab showed that spermatocytes from *Cntd1*$^{-/-}$ males show no synaptic defects (Gray et al., 2020; Holloway et al., 2014). To investigate if synaptic defects could explain

the early loss of primordial follicles in *Cntd1*$^{-/-}$ females, we analyzed synapsis in prophase I oocytes
305 from 18.5dpc *Cntd1*$^{-/-}$ females using antibodies against the synaptonemal complex markers SYCP1 (Synaptonemal complex protein-1) and SYCP3. Beginning in zygonema, SYCP1 transverse filaments zip the central and axial elements of the synaptonemal complex together (de Vries et al., 2005). Full synapsis is the defining feature of pachynema in all meiotic organisms. Defects in the ability for these proteins to assemble properly results in quality control checkpoint activation and
310 subsequent apoptosis at the end of prophase I (Hamer et al., 2008; Yuan et al., 2000).

SYCP1 localization in *Cntd1*$^{HA/HA}$ and *Cntd1*$^{HA/-}$ oocytes were normal in leptotene through diplotene-staged oocytes (Fig. 5A,B,D,E,G,H,J,K). As expected, SYCP1 colocalized completely with SYCP3 in pachytene-staged *Cntd1*$^{HA/HA}$ and *Cntd1*$^{HA/-}$ oocytes, and did not exhibit any asynaptic events (Fig. 5G, H). We observed that *Cntd1*$^{-/-}$ oocytes showed appropriate co-
315 localization of SYCP1 and SYCP3 throughout leptonema through diplonema (Fig. 5C, F, I, L) and did not differ compared to *Cntd1*$^{HA/HA}$ and *Cntd1*$^{HA/-}$ oocytes of the same corresponding stages (Fig. 5A-L). Upon further analysis, partiasynaptic events (synaptonemal complex with at least one fork or bubble) in *Cntd1*$^{-/-}$ pachytene-staged oocytes were not significant compared to *Cntd1*$^{HA/HA}$ pachytene oocytes (Fisher's Exact Test p=0.175). Together, these results indicate that loss of
320 *Cntd1* does not result in defects in DSB repair or synapsis, and the corresponding checkpoints are most likely not the cause of significant loss of oocytes.

DISCUSSION

325 Defects in crossover regulation can lead to absence of chiasmata during meiosis and subsequent aneuploidy of the resulting gametes (Hassold and Hunt, 2001; Hunt and Hassold, 2008). More specifically, such non-disjunction events are particularly prevalent in the first meiotic division in women, with an estimated up to 70% of oocytes being aneuploid, in comparison to only 3-5% of spermatocytes showing non-disjunction events (Hassold and Hunt, 2001; Hunt and
330 Hassold, 2008; Nagaoka et al., 2012). This sexual dimorphism in segregation errors can be traced in part back to defects in establishing sites of crossovers during pachynema of meiosis I. Cytological studies on human oocytes revealed that exchangeless chromosomes—synapsed homologous chromosomes lacking a crossover site—and crossovers placed at a unfavorable location are common and account for this high rate of mis-segregation (Hassold and Hunt, 2001;

335 Hassold et al., 2021; Nagaoka et al., 2012). Given these data, studies unraveling the molecular dynamics of crossover regulation in mammalian oocytes are crucial. However, the technical challenges associated with isolating oocytes at early developmental timepoints have hindered such studies in females, with male meiosis being considerably easier to investigate. The current study was aimed at understanding the function of one key regulator of crossover decisions, CNTD1, in
340 mammalian oogenesis. We sought to understand the role of CNTD1 in the regulation of crossover designation compared to analogous events in males to better understand the high rate of crossover failure in oocytes compared to spermatocytes.

Our data demonstrate the essential requirement for CNTD1 in crossover regulation during meiosis in female mice. Specifically, CNTD1 functions to ensure that class I COs are established,
345 leading to accurate segregation of chromosomes at the first meiotic division. We speculate that oocyte CNTD1 functions similarly to CNTD1 in spermatocytes to regulate the endonuclease activity of MutLγ at sites of crossovers (Gray et al. 2020). Future studies are aimed at understanding the specific activitiy of CNTD1 in regulating MutLγ, as well as determining the mechanism by which *Cntd1*$^{-/-}$ oocytes are eliminated, given the absence of defects in synapsis and
350 DSB formation. Further emphasis on female meiosis is likely to yield critical information that elucidates why mammalian oogenesis is so error prone.

CNTD1^{SF} is expressed in both mammalian spermatocytes and oocytes

The observation that CNTD1 exists solely as a short form in the testes of male mice was
355 unexpected, but provided a unique mechanism of action for mammalian CNTD1 that is distinct from its worm ortholog, COSA-1 (Gray et al., 2020). Studies presented here confirm this finding and further demonstrate that CNTD1^{SF} is the sole form of CNTD1 functioning in mammalian meiosis in both oocytes and spermatocytes. The current study and previous exploration of CNTD1 in male meiosis provides strong evidence for the predominance of CNTD1^{SF} and a cyclin-
360 independent function for CNTD1: (1) an antibody against HA (in *Cntd1-HA* expressing mice) that shows the presence of a single band for CNTD1 in mouse testis and ovary that is smaller than the predicted size of "full length" CNTD1; (2) our observation of CNTD1^{SF} predominance in mouse testis is confirmed by studies of Bondarieva *et al,* who show a single CNTD1 band that is indicative of short form size using their custom antibody against CNTD1 (Bondarieva et al., 2020); (3) our
365 previous yeast two-hybrid analysis demonstrates that CNTD1^{SF} fails to interact with any CDK,

while "full-length" CNTD1 can interact with several CDKs (Gray et al., 2020); and (4) IP-WB as well as IP-MS from mammalian testis lysate using anti-HA antibodies for IP and anti-CDK2 antibodies for WB fail to show an interaction between CNTD1 and CDK2 (Gray et al. 2020; Bondarieva et al. 2020). Thus, unlike COSA-1, mammalian CNTD1 exists as a short form that
370 lacks key features encoded by exons 1 and 2 of the mouse gene. These features include motifs that confer cyclin-like activity on the resulting protein. *In silico* analysis also indicates that transcripts encoding the CNTD1 short form exist in other species as well, including eutherian animals such as human, chimpanzee, koala, dog, and beaver (Gray et al., 2019).

The cyclin-dependent manner in which the long form of CNTD1 is predicted to function
375 requires its interaction with the crossover associated cyclin-dependent kinase CDK2 (Bondarieva et al., 2020; Gray et al., 2020). We find no evidence, either *in vivo* or via yeast two-hybrid assays, of an interaction between endogenous mouse testis CNTD1 and any CDK (Gray et al., 2020). However, yeast-two-hybrid assays from our lab and another showed that $CNTD1^{LF}$ interacts with CDK2 (Bondarieva et al., 2020; Gray et al., 2020). The phosphorylation target of a hypothetical
380 CNTD1/CDK2 complex was predicted to be HEI10 in order to regulate RNF212-associated crossover sites, however this has not been shown *in vivo* or *in vitro* (Palmer et al., 2020). By contrast, our previous analysis in male meiosis indicated that endogenous $CNTD1^{SF}$ interacts with the Replication Factor C (RFC) complex, possibly to recruit the Proliferating cell nuclear antigen (PCNA) clamp to chromosome cores (Gaubitz et al., 2022, 2020). During pachynema, PCNA may
385 then be essential for activating the endonuclease activity of MLH3 to facilitate subsequent crossover formation, although this role for PCNA has only been tested *in vitro* thus far (Cannavo et al., 2020; Kulkarni et al., 2020). Given these data, we speculate that CNTD1 regulates RFC-PCNA localization to sites of MutLγ during crossover designation in both mammalian spermatocytes and oocytes (Gray et al., 2020).

390

<u>*Cntd1* is essential for the formation of crossovers in mammalian oocytes.</u>

We describe herein the systematic progression of prophase I in oocytes from $Cntd1^{-/-}$ females compared to $Cntd1^{HA/HA}$ and $Cntd1^{HA/-}$ littermate controls for both synapsis and DSB repair (Fig. 4A-L, 5A-L). Early events of DSB repair, as observed through the accumulation of RAD51
395 appear normal, but with perhaps a very subtle delay in removal of RAD51 at pachynema (Fig. 4M). Additionally, synapsis appears normal in the absence of CNTD1 in comparison to

Cntd1$^{HA/HA}$ and *Cntd1*$^{HA/-}$ oocytes (Fig. 5G-I). By pachynema, however, there is a complete absence of the MutL homolog, MLH1, a defining feature of class I CO resolution in *Cntd1*$^{-/-}$ oocytes (Fig. 1G). The loss of all class I crossovers observed in *Cntd1*$^{-/-}$ females results in dramatic
400 loss of pairing of most homologs at diakinesis, concurrent with loss of 95% of all chiasmata compared to oocytes from *Cntd1*$^{HA/HA}$ and *Cntd1*$^{HA/-}$ females (Fig. 1I-K). The persistence of 1-2 residual bivalent chromosomes in diakinesis oocytes from *Cntd1*$^{-/-}$ animals is suggestive of an intact class II crossover pathway, catalyzed by the activity of the structure-specific endonuclease MUS81-EME1 (Holloway et al. 2008). The presence of these residual bivalents are also observed
405 in several *Mlh1* and *Mlh3* mutant mouse strains, further reinforcing the persistence of the class II pathway (Edelmann et al., 1996; Kan et al., 2008; Woods et al., 1999). Data from *Prr19* mutant oocytes show residual bivalents present at diakinesis, indicating that this crossover regulator is also not necessary for the class II pathway (Bondarieva et al., 2020). The role of other crossover regulator proteins such as RNF212and HEI10 in the class II crossover pathway in oocytes remains
410 unknown. Taken together, our data reveal that CNTD1 operates exclusively in the class I CO pathway impacting the accumulation of MLH1 and CDK2.

Loss of *Cntd1* results in a primary ovarian insufficiency phenotype.

At the end of prophase I, oocytes are arrested in dictyate until ovulation (Hassold et al.,
415 2021; Morelli and Cohen, 2005; Wang and Pepling, 2021). Dictyate arrested oocytes undergo folliculogenesis beginning in early post-natal life, when the somatic cells of the ovary reorganize into granulosa cells and surround the oocytes to form primordial follicles (Tingen et al., 2009). However, the majority of primordial follicles are lost soon after birth in a process called atresia, in which oocytes undergo apoptosis (Tingen et al., 2009). In humans, atresia leads to the loss of 6
420 million oocytes, with only roughly 750,000 remaining by 6 months of age (Baker, 1963). While atresia is a normal process in all mammals, there are also examples of certain pathologies that result in excessive loss of oocytes and follicles. The most severe example of this in humans is primordial ovarian insufficiency (POI), in which either an insufficient number of or defective oocytes in human females before the age of 40 can lead to infertility or difficulty with conception
425 (Guo et al., 2017; Huang et al., 2021; Ke et al., 2023; Veitia, 2020). The causes underlying POI are numerous; however, recent Next Generation Sequencing (NGS) studies have implicated several meiotic genes involved in DSB repair and synapsis, including, *MSH4*, *PRDM9*, *SYCE1,*

and *SLX4* (Baker, 1963; Huang et al., 2021; Ke et al., 2023). Moreover, extensive studies from the Schimenti lab to understand the checkpoint mechanism involved in follicle loss uncovered other
430 meiotic mouse mutants such as *Dmc1*, *Spo11*, *Trip13,* and *Hormad1* which also exhibit a POI-like phenotype, adding more evidence to defective DSB repair and synapsis triggering a quality control checkpoint (Bolcun-Filas et al., 2014; Di Giacomo et al., 2005; Rinaldi et al., 2020, 2017). The checkpoint kinase protein, CHK2, was found to be involved in the elimination of oocytes in these mutants (Bolcun-Filas et al., 2014; Rinaldi et al., 2020, 2017). More recent studies into the
435 crossover regulators *Rnf212*, *Hei10*, and *Prr19* show that folliculogenesis occurs in these mutants, however the extent of any defects in folliculogenesis remains unknown (Bondarieva et al., 2020; Qiao et al., 2014; Ward et al., 2007) . *Rnf212* mutant oocytes do not display any synaptic defects and further investigation unveiled an increase in oocyte number in mutants due to its role in ensuring oocyte quality (Qiao et al., 2018; Reynolds et al., 2013).

440 Studies reported herein demonstrate that loss of CNTD1 results in a dramatic depletion of oocytes that begins as early as PND1 (Figs. 3, 6), leading to a statistically significant decline by post-natal day 14 and continuting to increae up until adulthood when there is a concurrent loss of later stage (primary, secondary, and antral) follicles. This early loss of oocytes from birth is temporally distinct from oocyte loss phenotypes reported for other CO regulators, and is
445 inconsistent with the pachytene-staged appearance of CNTD1 and the phenotypic consequences of its loss beginning from pachynema onwards. To illustrate this, it is important to remember that loss of *Msh4* or *Msh5,* both of which result in defects from zygonema onwards, results in a similar timing of oocyte loss from birth, albeit much more dramatic and rapid (Edelmann et al., 1999; Kneitz et al., 2000) (Fig. 6). Mice lacking *Mlh1* or *Mlh3* have similar meiotic phenotypes to *Cntd1*$^{-/-}$
450 females, showing normal prophase I progression through until pachynema and loss of chiasmata at diakinesis (Woods et al. 1999; Kan et al. 2008) (Fig. 6). By contrast, however, loss of primordial follicles in *Mlh1*$^{-/-}$ and *Mlh3*$^{-/-}$ females does not result in the dramatic early loss of oocytes observed in *Cntd1*$^{-/-}$ females in the current study, and instead ovaries from adult *Mlh1*$^{-/-}$ and *Mlh3*$^{-/-}$ females are relatively normal in size and morphology (Kan et al., 2008; Lipkin et al., 2002; Woods et al.,
455 1999). To begin to understand the mechanism of early primordial loss in *Cntd1*$^{-/-}$ females, we hypothesized that a dual checkpoint mechanism involving unrepaired DSBs and/or defects in synapsis could be the cause. The dual-checkpoint model hypothesizes that both an elevation in unrepaired double-strand breaks (DSB) and persistent asynapsis beyond zygonema leads to the

accumulation of the DNA damage response factors and trigger the pachytene checkpoint leading to cell death (Bolcun-Filas et al., 2014; Ravindranathan et al., 2022; Rinaldi et al., 2020). Mammalian oocytes seem to be particularly tolerant of synapsis and DSB defects, as seen in the sexual dimorphism observed in *Sycp3* homozygous mutant mice (Kolas et al., 2004). Despite the significant loss of primordial follicles starting soon after birth, oocytes from *Cntd1*$^{-/-}$ animals do not show defects in synapsis or elevated RAD51 foci (Fig. 4E), thereby raising the question of how these oocytes are eliminated. In fact, we observed that *Cntd1*$^{-/-}$ oocytes were present at all stages of prophase I, indicating that *Cntd1* is not required for synapsis to progress efficiently (Fig. 4A-D). This result is consistent with observations of oocyte meiosis in *Rnf212*$^{-/-}$ females, which also show no defects in synapsis, implying these crossover regulators are unnecessary for synapsis (Reynolds et al., 2013).

Similar to the lack of synapsis defects in *Cntd1*$^{-/-}$ oocytes, we also observed no defects in early DSB processing, suggesting that unrepaired DSBs are also not the cause of oocyte loss in the absence of CNTD1. Future studies will investigate the role of the checkpoint kinase *Chk2* in oocyte quality control in crossover regulation, as this has been shown to be a predominant quality control regulator. Together, we speculate that *Cntd1* has a novel role in maintaining oocyte quality and its loss results in the apoptosis of oocytes after the dual DSB and synapsis checkpoint, at a time that is later in prophase I progression and/or early dictyate arrest. In mouse spermatocytes, CNTD1 has been proposed to play dual roles during meiosis: in promoting CO formation through an interaction with the RFC/PCNA complex, and in regulating meiotic cell cycle progression through an interaction with the SKP1-Cullin-F-box (SCF) ubiquitin ligase complex (Gray et al. 2020). It is possible the earlier loss of oocytes in *Cntd1* mutants compared to mutants of proteins similarly essential for Class I COs (*Mlh1/3, Hei10, Rnf212*) could point to a conserved role of CNTD1 in regulating meiotic cell cycle progression in both sexes, specifically the maintenance of dictyate arrest in oocytes and the prophase I to M-phase progression in spermatocytes.

In human meiocytes, the premature loss of oocytes is a trend that is well established, and is due to oocytes having extensive chromosomal defects that result from nondisjunction events (Hassold and Hunt, 2001; Hassold, 1986; Hassold et al., 2021; Wang et al., 2017). While there are many factors that lead to chromosome mis-segregation, previous modeling studies have suggested that crossover placement and maturation might underlie the error-prone phenotype that is commonly observed in females (Wang et al. 2017). Previous studies in the field have focused

490 almost exclusively on meiotic disruption in spermatogenesis, with only a handful of studies focused solely on oocytes, thereby leaving a large gap in knowledge into the crossover dynamics in oocytes. More broadly, how these oocytes are being lost in the context of crossover regulation has not been investigated in depth, with only one publication in *Rnf212* mutants showing disrupted DSB repair can trigger apoptosis (Qiao et al., 2018). Therefore, this study and previous oocyte-
495 focused studies have laid foundational groundwork in understanding a component of the regulation of crossovers in mammalian oocytes.

FIGURE LEGENDS

500

Figure 1. *Cntd1*$^{-/-}$ females lack class I crossovers and show a significant increase in univalent chromosomes. Localization of CNTD1-HA (green) and SYCP3 (magenta) in pachytene oocytes from (A) *Cntd1*$^{HA/HA}$, (B) *Cntd1*$^{HA/-}$, and (C) *Cntd1*$^{-/-}$ fetuses using antibodies against each protein raised in rabbit and mouse, respectively. Localization of MLH1 (green) and SYCP3 (magenta) in
505 pachytene oocytes from (E) *Cntd1*$^{HA/HA}$, (F) *Cntd1*$^{HA/-}$, and (G) *Cntd1*$^{-/-}$ females using antibodies against each protein raised in mouse and rabbit, respectively. (D) Quantification of HA foci in oocytes from *Cntd1*$^{HA/HA}$ (n=168), *Cntd1*$^{HA/-}$ (n=86), and *Cntd1*$^{-/-}$ (n=41 nuclei) females and (H) MLH1 foci in oocytes from *Cntd1*$^{HA/HA}$ (n=87), *Cntd1*$^{HA/-}$ (n=73) and *Cntd1*$^{-/-}$ (n=47 nuclei) females. Diakinesis preps with quantification in graphs, arrows indicate bivalents (red) and
510 univalent (blue). (I) *Cntd1*$^{HA/HA}$, (J) *Cntd1*$^{HA/-}$, and (K) *Cntd1*$^{-/-}$ chiasmata visualized with Giemsa staining. (L) Quantification of chiasmata for each genotype (*Cntd1*$^{HA/HA}$ n=8 cells, *Cntd1*$^{HA/-}$ n=11 cells, and *Cntd1*$^{-/-}$ n=9 cells) using a One-way ANOVA with Tukey's correction for multiple comparisons. P-values are as follows, * ($p<0.05$), ** ($p<0.01$), and *** ($p<0.001$), and **** ($p<0.0001$). Mean and standard deviation lines are in red. All experiments utilized $n \geq 3$ ovary
515 pairs per genotype.

Figure 2. CNTD1 exists in a short-form in fetal oocytes. Co-immunoprecipitation with anti-HA antibody in fetal ovary and adult testis lysate. (A) Western Blot against HA from IPs performed in
520 18.5dpc whole ovary lysate from *Cntd1*$^{HA/HA}$ and C57BL/6J females, and whole testis lysate from *Cntd1*$^{HA/HA}$ adult males. Approximately 40-100 ovaries from $n \geq 3$ fetuses were utilized per sample. Red arrows indicate the predicted mass of CNTD1 (~29.7kDa) in the elutions from fetal ovaries and adult testes from *Cntd1*$^{HA/HA}$ animals.

525 **Figure 3. Ovarian histology in *Cntd1*$^{HA/HA}$, *Cntd1*$^{HA/-}$, and *Cntd1*$^{-/-}$ females at different postnatal ages reveals a significant increase in the loss of primordial follicles.** (A-O) Histological sections of ovaries from *Cntd1*$^{HA/HA}$, *Cntd1*$^{HA/-}$, and *Cntd1*$^{-/-}$ female mice at post-natal day (PND) 1 (A-C), 14 (E-G), 28 (I-K), and adult (8-10 week) (M-O). Paraffin-embedded tissues were sectioned at 5 µm and stained with Hematoxylin and Eosin. Scale bars are equal to 100µm.

530 Quantification of primordial, primary, secondary, and antral follicles in ovaries at PND1 (D), PND14 (H), PND28 (L), and adult (P) ages from *Cntd1*$^{HA/HA}$, *Cntd1*$^{HA/-}$, and *Cntd1*$^{-/-}$ female mice. For each time point, follicles from n≥3 ovaries were quantified. One-way ANOVA with Tukey's multiple comparisons test. P-values are as follows: * p<0.05, ** p<0.01, and *** p<0.0001.

535 **Figure 4. Early DSB repair in *Cntd1*$^{-/-}$ oocytes is normal.** Localization of RAD51 (green) and SYCP3 (magenta) on chromosomes spreads from *Cntd1*$^{HA/HA}$, *Cntd1*$^{HA/-}$, and *Cntd1*$^{-/-}$ oocytes at leptonema (A-C), zygonema (D-F), pachynema (G-I), and diplonema (J-L). Using antibodies against each protein raised in rabbit and mouse, respectively. (M) Quantification of RAD51 in pachytene-staged cells, *Cntd1*$^{HA/HA}$ (n=78 nuclei), *Cntd1*$^{HA/-}$ (n=51 nuclei), *Cntd1*$^{-/-}$ (n=44 nuclei).
540 n ≥3 mice were used and data was analyzed using a One-way ANOVA with Tukey's multiple comparisons corrections test. P-values are as follows, * (p<0.05), ** (p<0.01), and *** (p<0.001), and **** (p<0.0001). Mean and standard deviation lines are in red.

Figure 5. Synapsis is unaltered in *Cntd1*$^{-/-}$ oocytes. Localization of SYCP1 (green) and SYCP3
545 (magenta) on chromosomes spreads from *Cntd1*$^{HA/HA}$, *Cntd1*$^{HA/-}$, and *Cntd1*$^{-/-}$ oocytes at leptonema (A-C), zygonema (D-F), pachynema (G-I), and diplonema (J-L). Using antibodies against each protein raised in rabbit and mouse, respectively.

Figure 6. Model of follicle loss in different meiotic mutants. Summary of known ovarian
550 phenotypes for genes important for CO designation and processing through the class I pathway. While some of the phenotypic consequences of these mutations have not been fully described, this summary represents our current understanding of the timing of loss of oocytes in each of the listed mutants. The position of each mutant on the line corresponds to the approximate timepoint of loss of oocytes in that mutant. Loss of oocytes in *Cntd1*$^{-/-}$ corresponds roughly to a timepoint after DSB,
555 DNA resection, and CO licensing factors (*Msh5, Dmc1, Spo11, Trip13*) but before CO maturation factors (*Rnf212, Mlh1, Mlh3, Hei10*). Data extacted from several sources (Bondarieva et al. 2020; Woods et al. 1999; Kan et al. 2008; Kneitz et al. 2000).

Supplementary Figure 1. Colocalization analysis of CNTD1 and MLH3. Representative
560 images of (A-C) *Cntd1*$^{HA/HA}$ (n=12 nuclei) and (E-G) *Cntd1*$^{HA/-}$ (n=19 nuclei) pachytene-staged

oocytes (n ≥ 3 fetal ovaries) stained for HA (magenta), MLH3 (green), and SYCP3 (blue). Images are representative of experiments from n ≥ 3 fetuses. Average percentage of colocalization for *Cntd1*$^{HA/HA}$ and *Cntd1*$^{HA/-}$ of MLH3 with HA is 91.53% and 87.34%, respectively. (D and H) Quantification of colocalization. Average percentage of colocalization for *Cntd1*$^{HA/HA}$ and
565 *Cntd1*$^{HA/-}$ of HA with MLH3 is 89.27% and 93.44%, respectively. Mean and standard deviation lines are in red.

Supplementary Figure 2. *Cntd1*$^{-/-}$ females are sterile. A 3 month trio breeding assay of *Cntd1*$^{HA/HA}$, *Cntd1*$^{HA/-}$, and *Cntd1*$^{-/-}$ females housed with a *Cntd1*$^{HA/HA}$ male. Total pup number per
570 litter are recorded for each dam genotype. n ≥ 3 females were used per genotype. Mean and standard deviation lines are in red. Litter sizes were analzed with a One-way ANOVA with Tukey's multiple comparisons corrections test. P-values are as follows, * ($p<0.05$), ** ($p<0.01$), and *** ($p<0.001$), and **** ($p<0.0001$). Mean and standard deviation lines are in red.

575 **AUTHOR CONTRIBUTIONS**

Experimental Design: Paula E. Cohen, Anna J. Wood, and Ian Wolff

Experiments: Anna J. Wood, Rania Ahmed, and Ian Wolff

Data analysis and Interpretation: Anna J. Wood, Rania Ahmed, Ian Wolff, Rachel Bradley, Paula E. Cohen

580 **Manuscript Preparation:** Anna J. Wood, Ian D. Wolff, and Paula E. Cohen

ACKNOWLEDGEMENTS

We extend our thanks to Dr. Stephen Gray, Dr. Maria De Las Mercedes Carro, Dr. Tegan Horan, Stephanie Tanis, Leah Simon, and Amanda Touey-May for their comments on the manuscript, and
585 to the entire Cohen lab for advice and guidance throughout the course of these studies. We also thank Dr. Carolline Ascenção for her experimental help with co-immunoprecipitations. We are exceptionally grateful to Eileen Shu for outstanding technical assistance and lab leadership. We thank the Cornell Stem Cell and Transgenic Core facility for the creation of the *Cntd1*$^{HA/HA}$ and *Cntd1*$^{-/-}$ mouse lines, Dr. Matthew Thomas from the Cornell Statistical Consulting Unit for his aid
590 in experimental design and data analysis, and the College of Veterinary Medicine Histology Core for tissue embedding and sectioning. Funding for this research was provided by the National

Institutes of Health through grants to P.E.C. (HD041012, HD097987), I.D.W. (F32HD106630), and through a scholarship from The Natural Sciences and Engineering Research Council of Canada to RAB (PGSD-577969).

595

DELCARATIONS OF INTERESTS

The authors declare no competing interests.

KEY RESOURCES TABLE

REAGENT or RESOURCE	SOURCE	IDENTIFIER
Antibodies		
HA (Rabbit monoclonal)	Cell Signaling	3724
MLH1 (mouse)	BD Pharmigen	554073
MLH3 (guinea pig)	Custom made	Lead contact
SYCP3 (rabbit)	Custom made	Lead contact
SYCP3 (mouse)	Abcam	
RAD51 (rabbit)	EMD Millipore	PC130-100UL
SYCP1 (rabbit)	Abcam	ab15090
HA-Tag Rabbit mAb (Magnetic Bead Conjugate)	Cell Signaling	11846
Goat anti-Rabbit IgG (H+L) Secondary Antibody, HRP	Thermo Scientific	31460
Alexa Fluor 488-AffiniPure F(ab')2 Fragment Goat Anti-Guinea Pig IgG (H+L)	Jackson ImmunoResearch	106-546-003
Alexa Fluor 488-AffiniPure F(ab')2 Fragment Goat Anti-Rabbit IgG	Jackson ImmunoResearch	111-546-046
Alexa Fluor 488-AffiniPure F(ab')2	Jackson ImmunoResearch	115-546-071

Fragment Goat Anti-Mouse IgG		
Alexa Fluor 594-conjugated AffiniPure F(ab')2 Fragment Goat Anti-Mouse IgG	Jackson ImmunoResearch	115-586-146
Alexa Fluor 594-AffiniPure F(ab')2 Fragment Goat Anti-Rabbit IgG	Jackson ImmunoResearch	111-586-046
Alexa Fluor 647-AffiniPure F(ab')2 Fragment Goat Anti-Mouse IgG	Jackson ImmunoResearch	115-606-071
Alexa Fluor 647-AffiniPure F(ab')2 Fragment Goat Anti-Rabbit IgG	Jackson ImmunoResearch	111-606-046
Alexa Fluor 647-AffiniPure F(ab')2 Fragment Goat Anti-Guinea Pig IgG	Jackson ImmunoResearch	106-606-003
Chemicals, peptides, and recombinant proteins		
Western blot and immunoprecipitations		
Laemmli buffer	BioRad	1610747 (4X) 1610737 (2X)
Pierce™ BCA Protein Assay Kit	ThermoFisher	23225

Pierce™ ECL Western Blotting Substrate	ThermoFisher	32106
SuperSignal™ West Pico PLUS Chemiluminescent Substrate	ThermoFisher	34580
SuperSignal™ West Femto Maximum Sensitivity Substrate	ThermoFisher	34096
30% Acrylamide/Bis Solution 37.5:1	BioRad	1610158
EveryBlot Blocking Buffer	BioRad	12010010
Trans-Blot Turbo 5X Transfer Buffer	BioRad	10026938
TMED	BioRad	161-0801
2,2,2-Trichloroethanol	Sigma-Aldrich	T54801-100G
10X Tris/Glycine/SDS Buffer	BioRad	1610772
Roche complete EDTA-free protease inhibitor tablet	Sigma-Aldrich	1873580001
Chiasmata spreads		
KSOM medium	Sigma-Aldrich	MR-101-D
Light mineral oil	Millipore Sigma	ES-005-C

Micropipettes	CooperSurgical Inc.	MXL3-150
Sodium citrate	Fisher Scientific	S279-500
Methanol	Fisher Scientific	A412-4
Acetic acid, Glacial	Fisher Scientific	A38-212
Giemsa stain	Sigma	GS500-500L
Permount	Fisher Scientific	SP15100
EmbryoMax M2 Medium	Millipore Sigma	MR-015-D
Microscope slides	Fisher Scientific	12-544-2
Milrinone	Sigma-Aldrich	M4659-10MG
Histology and follicle quantification		
Harris Hematoxylin	Fisher Scientific	NC9520196
Eosin-Y-Solution	Fisher Scientific	E511-25
Safeclear (Histoclear)	Fisher Scientific	23-044-192
Epredia Shadon Bluing Reagent	Fisher Scientific	6769002
Permount	Fisher Scientific	SP15-100
Bouin's Solution	Sigma-Aldrich	HT10132-1L
Histogel	Fisher Scientific	NC9150318
Fetal oocyte spreads		
Paraformaldehyde	Electron Microscopy Sciences	19200
Kodak Professional Photo-Flo 200	Kodak	1464510
Goat serum, New Zealand origin	ThermoFisher Scientific	16210072
Microscope slides, 6 well, 8mm	Laborimpex (VWR)	63423-08 (100490-336)

Standard coverslips #1.5	VWR	152460 (16002-268)
Bovine Serum Albumin	Sigma-Aldrich	A7906-500g
TritonX-100	Fisher Scientific	BP151-500
	Experimental models: organisms and strains	
C57BL6/J	The Jackson Laboratory	#000664
Cntd1^{HA}	Doi:10.1016/j.celrep.2020.107858	Lead contact
	Oligonucleotides (Genotyping)	
Cntd1_HA_Fwd	5'-GCGCACGAGTGTTTGTGCACT-3'	IDT
Cntd1_HA_Rev	5'-CCAGTGACAAGGCAGTGCGGGTCAGCC-3'	IDT

RESOURCE AVAILABILITY

Lead contact

Further information and requests for resources and reagents should be directed to and will be fulfilled by the Lead Contact, Paula Cohen (paula.cohen@cornell.edu)

Materials Availability

Mouse lines generated within this study are available upon request from the Lead Contact, Paula Cohen (paula.cohen@cornell.edu)

Data and Code availability

This study did not generate any code.

METHODS

Mouse strains

615 All mouse strains were maintained on a C57BL6/J background. *Cntd1*^{HA} and *Cntd1*$^{-/-}$ mouse strains were used as reported previously (Gray et al., 2020). All mice were maintained under strictly defined conditions of constant temperature and light:day cycles, with food and water *ad libitum.* Animal handling and procedures were performed following approval by the Cornell Institutional Animal Care and Use Committee, under protocol 2004-0063. All experimental 620 animals were genotyped from ear snips collected and processed with 0.05M NaOH and 1M Tris-HCl pH 7.2. A PCR was performed using the following primers:

Cntd1_HA_Fwd: 5'-GCGCACGAGTGTTTGTGCACT-3'

Cntd1_HA_Rev: 5'-CCAGTGACAAGGCAGTGCGGGTCAGCC-3'.

The genotype was determined from a 1.5% Agarose RA gel for animals containing the FLAG-HA 625 allele (~327bp), or the mutant allele (~273bp).

Breeding assay

Two *Cntd1*$^{HA/HA}$, *Cntd1*$^{HA/-}$, or *Cntd1*$^{-/-}$ females and one *Cntd1*$^{HA/HA}$ male were allowed to mate for up to 3 months. Each trio was allowed to produce pups up to three months from the pairing 630 date. Subsequent litter numbers were recorded at weaning.

Chromosome spreading and immunofluorescence

Oocytes were isolated from 16.5 to 18.5 days post-coitum (dpc), with the day of observing the vaginal plug being 0.5 dpc. Ovaries were dissected into 1X PBS and incubated in hypotonic extraction buffer (HEB) for approximately 20-30 minutes at room temperature, which comprised 635 of Tris-HCl (pH 8.2), 50 mM sucrose, 17 mM trisodium dihydrate, 5 mM EDTA, 0.5mM DTT, and 0.1 mM PMSF. After incubation the ovaries were punctured in 100 mM sucrose and added to slides containing 1% paraformaldehyde with 20% Triton-X. The ovaries were allowed to fix at room temperature for 2 hours in a humid chamber. After 2 hours, slides were allowed to dry at room temperature. Slides were washed in a mixture of 0.4% Photoflo and miliQ-H_2O once for 5 640 minutes then allowed to dry completely. For preparation for primary antibody staining, slides were washed with 0.4% Photoflo in 1X PBS once for 10 minutes. This was followed by washing in a Triton wash comprised of 0.5% Triton and 10% Antibody Dilution Buffer ("ADB": 3g BSA,

90mL 1X PBS, and 20% Triton-X, filter sterilized) in 1X PBS once for 10 minutes followed by blocking in 10% ADB in 1X PBS for 30 minutes at room temperature. Slides were subsequently
645 stained with the antibody of interest (HA 1:500, MLH1 1:50, SYCP3 [mouse] 1:500, MLH3 [guinea pig] 1:500, SYCP3 [rabbit] 1:1000, RAD51 1:500, SYCP1 [rabbit] 1: 5000) overnight at room temperature in a humid chamber. The following day, slides were washed with 0.4% Photoflo in 1X PBS, Triton wash, and blocked in 1X ADB as stated above. Secondary Alexa-fluor antibodies were diluted 1:2000 in 10X ADB and slides were stained for 2 hours at room
650 temperature. Following secondary antibody staining, slides were washed in the dark in 0.4% Photoflo in 1X PBS (three 5-minute washs) at room temperature, followed by a wash in 0.4% Photoflo in miliQ-H_2O once for 5 minutes. Slides were allowed to dry and mounted with DAPI plus Antifade (8 ng/mL) and sealed with rubber cement and imaged.

Ovary Histology and quantification

655 One ovary from mice at postnatal days 1, 14, and 28, and 8–12-week-old adults were fixed in Bouin's or Formalin for 4 hours at room temperature on a nutator. Following fixation, ovaries were washed in 70% ethanol. For histological preparation, ovaries were embedded in Histogel before being prepared in a cassette. The Cornell Histopathology core serial sectioned Histogel and paraffin embedded ovaries in 5 micrometer sections. Hematoxylin and Eosin staining were
660 performed as follows: three 5-minute washes in Histoloclear, followed by three 3-minute washes in 95% ethanol, subsequently followed by one 5 minute wash in 80% ethanol and 70% ethanol, with a final wash in 1X PBS for 10 minutes. Staining comprised of one 30-second staining in Hematoxylin followed by two washes in miliQ-H_2O, followed by two dunks in Bluing reagent and subsequent washes in miliQ-H_2O. Slides were stained with Eosin for 2 minutes followed by four
665 dunks in miliQ- H_2O. Slides were then processed through 1 dunk of 70% ethanol and 80% ethanol, and three 3-minute washes in 95% ethanol, finished with three 3-minute Histoclear washes. Slides were dried and mounted with Permount and subsequently imaged. Sections were imaged on Aperio software using an Aperio CS2 Digital Pathology Slide Scanner microscope. The total number of follicles was determined by multiplying the raw counts from every fifth section by 5 to correct for
670 the sections not counted. Follicles were staged as explained previously and follicles with oocytes without a visible nucleus were excluded from quantification to avoid double counting (Sarma et al., 2020).

Oocyte metaphase spread preparations.

675 Spreads were prepared as previously described in Sun and Cohen (Sun and Cohen, 2013). Briefly, M2 collection media was made comprised of Waymouth's medium, FBS, 1% Pennicillin-Streptomycin, and 2.5 mg/mL Sodium Pyruvate. A 60 mm plastic petri dish was prepared with 20 *μL* KSOM droplets and Light Mineral oil covering the droplets. Collection media and the KSOM droplets with light mineral oil were equilibrated overnight in a 37°C incubator (5% CO_2). Ovaries
680 from unstimulated female mice aged 24-28 days were collected directly into warmed collection media. The ovaries were punctured using 26 gauge needles to release oocytes. Oocytes with a visible zona pellucida and cumulus cells were collected using a 150-striper tip and placed into one of the KSOM droplets. Dissociation of the cumulus cells was achieved by mouth pipetting oocytes through the KSOM droplets until cumulus cells were gone. Oocytes in KSOM and mineral oil
685 were incubated for approximately 7-8 hours until the oocytes entered metaphase I. Oocytes were moved to 20 μL droplets of 1% hypotonic solution (1g sodium citrate dissolved in 100 mL miliQ-H_2O) for 15 minutes. A glass slide prepared with a China pen or hydrophobic pen in a grid formation were used. 1-2 μL of hypotonic solution was placed onto one square on the glass slide. Oocytes without the zona pellucida were transferred to the drop. Excess hypotonic solution was
690 siphoned off to allow the oocytes to adhere to the slide. One drop of Carnoy's fixative (3 parts methanol and 1-part glacial acetic acid) was added directly onto the oocytes. The fixative was allowed to disperse, followed by another 1-2 drops of Carnoy's fixative. The slides were allowed to air dry. This was followed by Giemsa staining (48 mL miliQ-H_2O and 2 mL Giemsa) in a coplin jar for 3 minutes. The slides were washed 3 x 3 minutes in miliQ-H_2O. The slides were allowed to
695 dry at room temperature, immediately followed by mounting with Permount and a coverslip. Chiasmata were imaged at 63X.

Oocyte co-immunoprecipitations

Co-immunoprecipitations were performed as reported previously with modifications (Gray et al.,
700 2020). Approximately 40 ovaries per genotype (*Cntd1*$^{HA/HA}$ or C57BL6/J) from 18.5 dpc embryos were isolated and snap frozen on dry ice, then stored at -80°C until use. *Cntd1*$^{HA/HA}$ testes were collected from 10 week old adults, detunicated, and snap frozen on dry ice before storage at -80°C until use. Ovaries or testis were added to 1 mL of cold lysis buffer (50 mM Tris-HCl pH 8.0, 0.2%

NP-40, 150 mM NaCl, 5 mM EDTA, 0.1 mg/mL PMSF, Roche complete EDTA-free protease
705 inhibitor tablet) and sonicated with the following parameters: 23% amplitude for 12 seconds, 0.4 seconds on / 0.2 seconds off, and rest on ice for approximately 30 seconds between runs. Sonicated tissues were then spun down at 15,000 x g for 20 minutes at 4°C and the supernatant was collected. 20 µL of lysate was removed for BCA quantification and protein amounts were quantified based on manufacturer protocol. 10 µL of rabbit anti-HA conjugated magnetic beads were added to 500
710 µL of lysate (250 µg total protein) and incubated overnight at 4°C. Unbound supernatant was removed from beads, and beads were washed 4 times for 5 minutes in 500µL ice cold wash buffer (lysis buffer with 250 mM NaCl). Beads were then resuspended in 100µL of wash buffer and transferred to a fresh tube. Bound proteins were eluted from beads by resuspending in 30µL elution buffer (100 mM Tris-HCl pH 8.0, 1% SDS, and 10 mM DTT) then incubating at 65°C for 15
715 minutes. Elutant was then collected, added to 10 µL 4X Laemmli sample buffer and boiled for 5 minutes at 95°C. Input gel samples were taken before addition of HA beads: 30 µL of lysate was added to 10 µL 4X Laemmli sample buffer (BioRad) and boiled at 95°C for 5 minutes.

SDS-PAGE and Western Blotting

720 Protein samples were separated by SDS-PAGE on gels varying in percentage from 6%–14% and transferred to methanol activated PVDF membranes using a Biorad Mini Trans-Blot Cell. Membranes were blocked by incubating in EveryBlot Blocking Buffer at room temperature while rotating at 60 rpm for 10 minutes. Membranes were then incubated overnight in primary antibody diluted in EveryBlot Blocking Buffer at 4°C. Membranes were washed three times in 0.1% TBST
725 and subsequently incubated with secondary antibody for 2 hours at room temperature, followed by three 0.1% TBST washes. Membranes were developed using various ECL reagents and imaged using a Biorad ChemiDoc imager. Antibodies used in this study are described in the Key Resources Table.

730 **Image acquisition**

Imaging was performed using a Zeiss Axiophot Z1 microscope attached to a cooled charge-coupled device (CCD) Black and White Camera (Zeiss McM). Images were captured and pseudo-colored using ZEN 3.0 software (Carl Zeiss AG, Oberkochen. Germany). The brightness and

contrast of images were adjusted using ImageJ (Schindelin et al. 2012)(National Institutes of Health, USA).

QUANTIFICATION AND STATISTICAL ANALYSIS

Statistical analyses were performed using GraphPad Prism version 9.00 for Macintosh and Microsoft Excel. Specific analyses are described within the text and the corresponding figures. All analyses used a One-Way ANOVA with a Tukey's multiple comparisons correction and the alpha value was established at 0.05. All statistical analysis was monitored by the Cornell Statistical Consulting Unit.

745 **LITERATURE CITED**

Baker TG. 1963. A quantitative and cytological study of germ cells in human ovaries. *Proceedings of the Royal Society of London, Series B, Biological Sciences* **158**:417–433.

Bolcun-Filas E, Rinaldi VD, White ME, Schimenti JC. 2014. Reversal of female infertility by Chk2 ablation reveals the oocyte DNA damage checkpoint pathway. *Science* **343**:533–536.
750 doi:10.1126/science.1247671

Bondarieva A, Raveendran K, Telychko V, Rao HBDP, Ravindranathan R, Zorzompokou C, Finsterbusch F, Dereli I, Papanikos F, Tränkner D, Schleiffer A, Fei J-F, Klimova A, Ito M, Kulkarni DS, Roeder I, Hunter N, Tóth A. 2020. Proline-rich protein PRR19 functions with cyclin-like CNTD1 to promote meiotic crossing over in mouse. *Nat Commun* **11**:3101.
755 doi:10.1038/s41467-020-16885-3

Cannavo E, Sanchez A, Anand R, Ranjha L, Hugener J, Adam C, Acharya A, Weyland N, Aran-Guiu X, Charbonnier J-B, Hoffmann ER, Borde V, Matos J, Cejka P. 2020. Regulation of the MLH1-MLH3 endonuclease in meiosis. *Nature* **586**:618–622. doi:10.1038/s41586-020-2592-2

760 Cao L, Alani E, Kleckner N. 1990. A pathway for generation and processing of double-strand breaks during meiotic recombination in S. cerevisiae. *Cell* **61**:1089–1101. doi:10.1016/0092-8674(90)90072-m

Cloud V, Chan Y-L, Grubb J, Budke B, Bishop DK. 2012. Rad51 is an accessory factor for Dmc1-mediated joint molecule formation during meiosis. *Science* **337**:1222–1225.
765 doi:10.1126/science.1219379

de Vries FAT, de Boer E, van den Bosch M, Baarends WM, Ooms M, Yuan L, Liu J-G, van Zeeland AA, Heyting C, Pastink A. 2005. Mouse *Sycp1* functions in synaptonemal complex assembly, meiotic recombination, and XY body formation. *Genes Dev* **19**:1376–1389. doi:10.1101/gad.329705

770 de Vries SS, Baart EB, Dekker M, Siezen A, de Rooij DG, de Boer P, te Riele H. 1999. Mouse MutS-like protein Msh5 is required for proper chromosome synapsis in male and female meiosis. *Genes Dev* **13**:523–531. doi:10.1101/gad.13.5.523

Di Giacomo M, Barchi M, Baudat F, Edelmann W, Keeney S, Jasin M. 2005. Distinct DNA-damage-dependent and -independent responses drive the loss of oocytes in recombination-
775 defective mouse mutants. *Proc Natl Acad Sci USA* **102**:737–742. doi:10.1073/pnas.0406212102

Edelmann W, Cohen PE, Kane M, Lau K, Morrow B, Bennett S, Umar A, Kunkel T, Cattoretti G, Chaganti R, Pollard JW, Kolodner RD, Kucherlapati R. 1996. Meiotic pachytene arrest in MLH1-deficient mice. *Cell* **85**:1125–1134. doi:10.1016/s0092-8674(00)81312-4

780 Edelmann W, Cohen PE, Kneitz B, Winand N, Lia M, Heyer J, Kolodner R, Pollard JW, Kucherlapati R. 1999. Mammalian MutS homologue 5 is required for chromosome pairing in meiosis. *Nat Genet* **21**:123–127. doi:10.1038/5075

Gaubitz C, Liu X, Magrino J, Stone NP, Landeck J, Hedglin M, Kelch BA. 2020. Structure of the human clamp loader reveals an autoinhibited conformation of a substrate-bound AAA+
785 switch. *Proc Natl Acad Sci USA* **117**:23571–23580. doi:10.1073/pnas.2007437117

Gaubitz C, Liu X, Pajak J, Stone NP, Hayes JA, Demo G, Kelch BA. 2022. Cryo-EM structures reveal high-resolution mechanism of a DNA polymerase sliding clamp loader. *eLife* **11**. doi:10.7554/eLife.74175

Gray S, Cohen PE. 2016. Control of meiotic crossovers: from double-strand break formation to
790 designation. *Annu Rev Genet* **50**:175–210. doi:10.1146/annurev-genet-120215-035111

Gray S, Santiago E, Chappie JS, Cohen PE. 2019. Cyclin N-Terminal Domain-Containing 1 (CNTD1) coordinates meiotic crossover formation with cell cycle progression in a cyclin-independent manner. *BioRxiv*. doi:10.1101/750596

Gray S, Santiago ER, Chappie JS, Cohen PE. 2020. Cyclin N-Terminal Domain-Containing-1
795 Coordinates Meiotic Crossover Formation with Cell-Cycle Progression in a Cyclin-Independent Manner. *Cell Rep* **32**:107858. doi:10.1016/j.celrep.2020.107858

Gruhn JR, Rubio C, Broman KW, Hunt PA, Hassold T. 2013. Cytological studies of human meiosis: sex-specific differences in recombination originate at, or prior to, establishment of double-strand breaks. *PLoS ONE* **8**:e85075. doi:10.1371/journal.pone.0085075

800 Guo T, Zhao Shidou, Zhao Shigang, Chen M, Li G, Jiao X, Wang Z, Zhao Y, Qin Y, Gao F, Chen Z-J. 2017. Mutations in MSH5 in primary ovarian insufficiency. *Hum Mol Genet* **26**:1452–1457. doi:10.1093/hmg/ddx044

Hamer G, Wang H, Bolcun-Filas E, Cooke HJ, Benavente R, Höög C. 2008. Progression of meiotic recombination requires structural maturation of the central element of the
805 synaptonemal complex. *J Cell Sci* **121**:2445–2451. doi:10.1242/jcs.033233

Hassold T, Hunt P. 2001. To err (meiotically) is human: the genesis of human aneuploidy. *Nat Rev Genet* **2**:280–291. doi:10.1038/35066065

Hassold T, Maylor-Hagen H, Wood A, Gruhn J, Hoffmann E, Broman KW, Hunt P. 2021. Failure to recombine is a common feature of human oogenesis. *Am J Hum Genet* **108**:16–24.
810 doi:10.1016/j.ajhg.2020.11.010

Hassold TJ. 1986. Chromosome abnormalities in human reproductive wastage. *Trends in Genetics* **5**:105–110.

Haversat J, Woglar A, Klatt K, Akerib CC, Roberts V, Chen S-Y, Arur S, Villeneuve AM, Kim Y. 2022. Robust designation of meiotic crossover sites by CDK-2 through phosphorylation of the MutSγ complex. *Proc Natl Acad Sci USA* **119**:e2117865119. doi:10.1073/pnas.2117865119

Holloway JK, Booth J, Edelmann W, McGowan CH, Cohen PE. 2008. MUS81 generates a subset of MLH1-MLH3-independent crossovers in mammalian meiosis. *PLoS Genet* **4**:e1000186. doi:10.1371/journal.pgen.1000186

Holloway JK, Sun X, Yokoo R, Villeneuve AM, Cohen PE. 2014. Mammalian CNTD1 is critical for meiotic crossover maturation and deselection of excess precrossover sites. *J Cell Biol* **205**:633–641. doi:10.1083/jcb.201401122

Huang C, Guo T, Qin Y. 2021. Meiotic recombination defects and premature ovarian insufficiency. *Front Cell Dev Biol* **9**:652407. doi:10.3389/fcell.2021.652407

Hunt PA, Hassold TJ. 2008. Human female meiosis: what makes a good egg go bad? *Trends Genet* **24**:86–93. doi:10.1016/j.tig.2007.11.010

Hwang GH, Hopkins JL, Jordan PW. 2018. Chromatin Spread Preparations for the Analysis of Mouse Oocyte Progression from Prophase to Metaphase II. *J Vis Exp* **132**:e56736. doi:10.3791/56736

Kan R, Sun X, Kolas NK, Avdievich E, Kneitz B, Edelmann W, Cohen PE. 2008. Comparative analysis of meiotic progression in female mice bearing mutations in genes of the DNA mismatch repair pathway. *Biol Reprod* **78**:462–471. doi:10.1095/biolreprod.107.065771

Ke H, Tang S, Guo T, Hou D, Jiao X, Li S, Luo W, Xu B, Zhao S, Li G, Zhang X, Xu S, Wang L, Wu Y, Wang J, Zhang F, Qin Y, Jin L, Chen Z-J. 2023. Landscape of pathogenic mutations in premature ovarian insufficiency. *Nat Med* **29**:483–492. doi:10.1038/s41591-022-02194-3

Kneitz B, Cohen PE, Avdievich E, Zhu L, Kane MF, Hou H, Kolodner RD, Kucherlapati R, Pollard JW, Edelmann W. 2000. MutS homolog 4 localization to meiotic chromosomes is required for chromosome pairing during meiosis in male and female mice. *Genes Dev* **14**:1085–1097.

Kolas NK, Svetlanov A, Lenzi ML, Macaluso FP, Lipkin SM, Liskay RM, Greally J, Edelmann W, Cohen PE. 2005. Localization of MMR proteins on meiotic chromosomes in mice indicates distinct functions during prophase I. *J Cell Biol* **171**:447–458. doi:10.1083/jcb.200506170

Kolas NK, Yuan L, Hoog C, Heng HHQ, Marcon E, Moens PB. 2004. Male mouse meiotic chromosome cores deficient in structural proteins SYCP3 and SYCP2 align by homology but fail to synapse and have possible impaired specificity of chromatin loop attachment. *Cytogenet Genome Res* **105**:182–188. doi:10.1159/000078188

Kulkarni DS, Owens SN, Honda M, Ito M, Yang Y, Corrigan MW, Chen L, Quan AL, Hunter N. 2020. PCNA activates the MutLγ endonuclease to promote meiotic crossing over. *Nature* **586**:623–627. doi:10.1038/s41586-020-2645-6

Lenzi ML, Smith J, Snowden T, Kim M, Fishel R, Poulos BK, Cohen PE. 2005. Extreme heterogeneity in the molecular events leading to the establishment of chiasmata during meiosis i in human oocytes. *Am J Hum Genet* **76**:112–127. doi:10.1086/427268

Lipkin SM, Moens PB, Wang V, Lenzi M, Shanmugarajah D, Gilgeous A, Thomas J, Cheng J, Touchman JW, Green ED, Schwartzberg P, Collins FS, Cohen PE. 2002. Meiotic arrest and aneuploidy in MLH3-deficient mice. *Nat Genet* **31**:385–390. doi:10.1038/ng931

Morelli MA, Cohen PE. 2005. Not all germ cells are created equal: aspects of sexual dimorphism in mammalian meiosis. *Reproduction* **130**:761–781. doi:10.1530/rep.1.00865

Nagaoka SI, Hassold TJ, Hunt PA. 2012. Human aneuploidy: mechanisms and new insights into an age-old problem. *Nat Rev Genet* **13**:493–504. doi:10.1038/nrg3245

Palmer N, Talib SZA, Singh P, Goh CMF, Liu K, Schimenti JC, Kaldis P. 2020. A novel function for CDK2 activity at meiotic crossover sites. *PLoS Biol* **18**:e3000903. doi:10.1371/journal.pbio.3000903

Pittman DL, Cobb J, Schimenti KJ, Wilson LA, Cooper DM, Brignull E, Handel MA, Schimenti JC. 1998. Meiotic prophase arrest with failure of chromosome synapsis in mice deficient for Dmc1, a germline-specific RecA homolog. *Mol Cell* **1**:697–705. doi:10.1016/s1097-2765(00)80069-6

Qiao H, Prasada Rao HBD, Yang Y, Fong JH, Cloutier JM, Deacon DC, Nagel KE, Swartz RK, Strong E, Holloway JK, Cohen PE, Schimenti J, Ward J, Hunter N. 2014. Antagonistic roles of ubiquitin ligase HEI10 and SUMO ligase RNF212 regulate meiotic recombination. *Nat Genet* **46**:194–199. doi:10.1038/ng.2858

Qiao H, Rao HBDP, Yun Y, Sandhu S, Fong JH, Sapre M, Nguyen M, Tham A, Van BW, Chng TYH, Lee A, Hunter N. 2018. Impeding DNA break repair enables oocyte quality control. *Mol Cell* **72**:211-221.e3. doi:10.1016/j.molcel.2018.08.031

Ravindranathan R, Raveendran K, Papanikos F, San-Segundo PA, Tóth A. 2022. Chromosomal synapsis defects can trigger oocyte apoptosis without elevating numbers of persistent DNA breaks above wild-type levels. *Nucleic Acids Res* **50**:5617–5634. doi:10.1093/nar/gkac355

Reynolds A, Qiao H, Yang Y, Chen JK, Jackson N, Biswas K, Holloway JK, Baudat F, de Massy B, Wang J, Höög C, Cohen PE, Hunter N. 2013. RNF212 is a dosage-sensitive regulator of crossing-over during mammalian meiosis. *Nat Genet* **45**:269–278. doi:10.1038/ng.2541

Rinaldi VD, Bloom JC, Schimenti JC. 2020. Oocyte Elimination Through DNA Damage Signaling from CHK1/CHK2 to p53 and p63. *Genetics* **215**:373–378. doi:10.1534/genetics.120.303182

Rinaldi VD, Bolcun-Filas E, Kogo H, Kurahashi H, Schimenti JC. 2017. The DNA damage checkpoint eliminates mouse oocytes with chromosome synapsis failure. *Mol Cell* **67**:1026-1036.e2. doi:10.1016/j.molcel.2017.07.027

Sarma UC, Winship AL, Hutt KJ. 2020. Comparison of methods for quantifying primordial follicles in the mouse ovary. *J Ovarian Res* **13**:121. doi:10.1186/s13048-020-00724-6

Sun X, Cohen PE. 2013. Studying recombination in mouse oocytes. *Methods Mol Biol* **957**:1–18. doi:10.1007/978-1-62703-191-2_1

Tingen CM, Bristol-Gould SK, Kiesewetter SE, Wellington JT, Shea L, Woodruff TK. 2009. Prepubertal primordial follicle loss in mice is not due to classical apoptotic pathways. *Biol Reprod* **81**:16–25. doi:10.1095/biolreprod.108.074898

Toledo M, Sun X, Brieño-Enríquez MA, Raghavan V, Gray S, Pea J, Milano CR, Venkatesh A, Patel L, Borst PL, Alani E, Cohen PE. 2019. A mutation in the endonuclease domain of mouse MLH3 reveals novel roles for MutLγ during crossover formation in meiotic prophase I. *PLoS Genet* **15**:e1008177. doi:10.1371/journal.pgen.1008177

Veitia RA. 2020. Primary ovarian insufficiency, meiosis and DNA repair. *Biomed J* **43**:115–123. doi:10.1016/j.bj.2020.03.005

Wang S, Hassold T, Hunt P, White MA, Zickler D, Kleckner N, Zhang L. 2017. Inefficient crossover maturation underlies elevated aneuploidy in human female meiosis. *Cell* **168**:977-989.e17. doi:10.1016/j.cell.2017.02.002

Wang X, Pepling ME. 2021. Regulation of meiotic prophase one in mammalian oocytes. *Front Cell Dev Biol* **9**:667306. doi:10.3389/fcell.2021.667306

Ward JO, Reinholdt LG, Motley WW, Niswander LM, Deacon DC, Griffin LB, Langlais KK, Backus VL, Schimenti KJ, O'Brien MJ, Eppig JJ, Schimenti JC. 2007. Mutation in mouse *Hei10*, an e3 ubiquitin ligase, disrupts meiotic crossing over. *PLoS Genet* **3**:e139. doi:10.1371/journal.pgen.0030139

Woods LM, Hodges CA, Baart E, Baker SM, Liskay M, Hunt PA. 1999. Chromosomal influence on meiotic spindle assembly: abnormal meiosis I in female Mlh1 mutant mice. *J Cell Biol* **145**:1395–1406. doi:10.1083/jcb.145.7.1395

Yokoo R, Zawadzki KA, Nabeshima K, Drake M, Arur S, Villeneuve AM. 2012. COSA-1 reveals robust homeostasis and separable licensing and reinforcement steps governing meiotic crossovers. *Cell* **149**:75–87. doi:10.1016/j.cell.2012.01.052

Yoshida K, Kondoh G, Matsuda Y, Habu T, Nishimune Y, Morita T. 1998. The mouse RecA-like gene Dmc1 is required for homologous chromosome synapsis during meiosis. *Mol Cell* **1**:707–718. doi:10.1016/s1097-2765(00)80070-2

Yuan L, Liu JG, Zhao J, Brundell E, Daneholt B, Höög C. 2000. The murine *Scp3* gene is
920 required for synaptonemal complex assembly, chromosome synapsis, and male fertility. *Mol Cell* **5**:73–83. doi:10.1016/S1097-2765(00)80404-9

Wood et al., Figure 1.

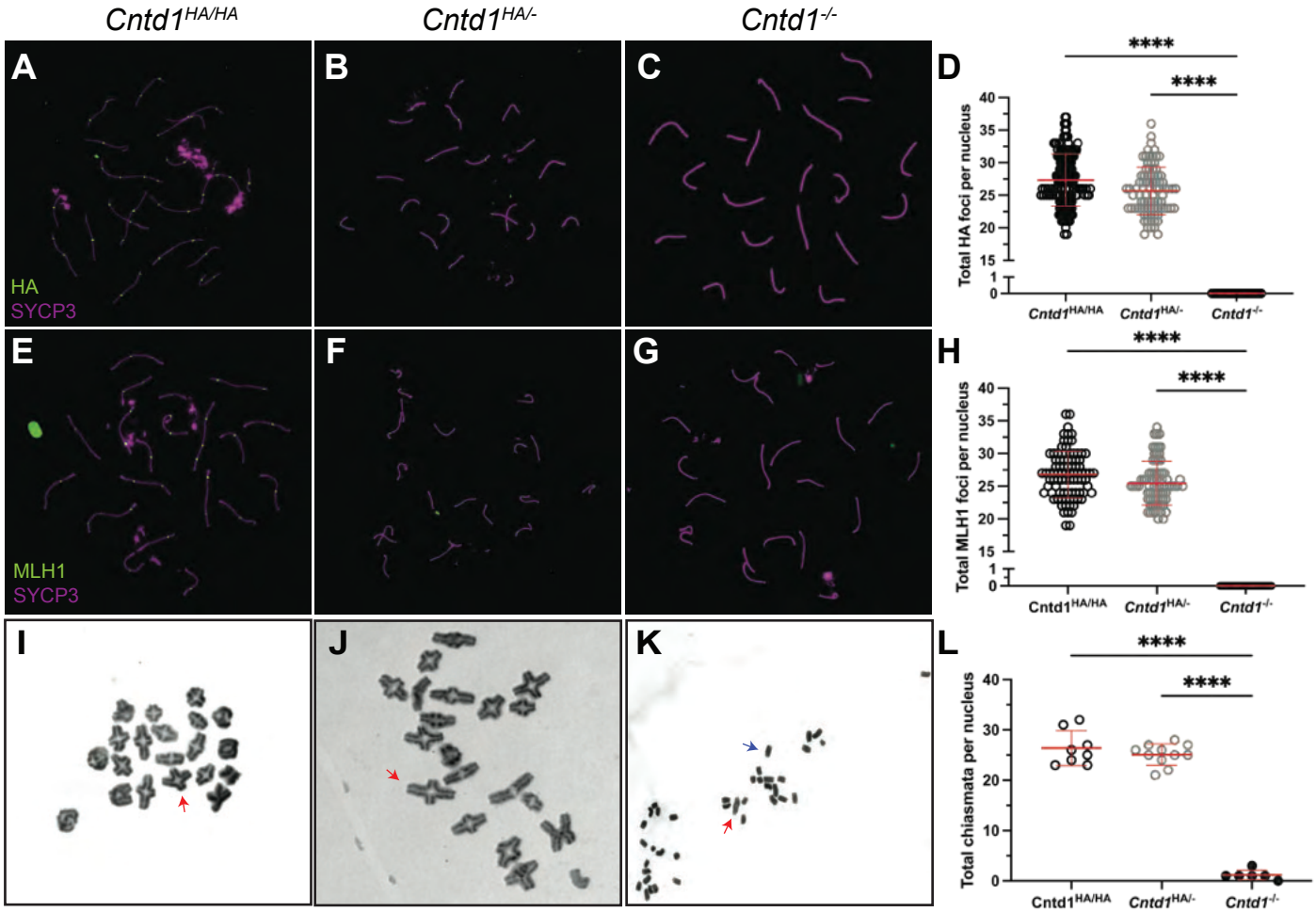

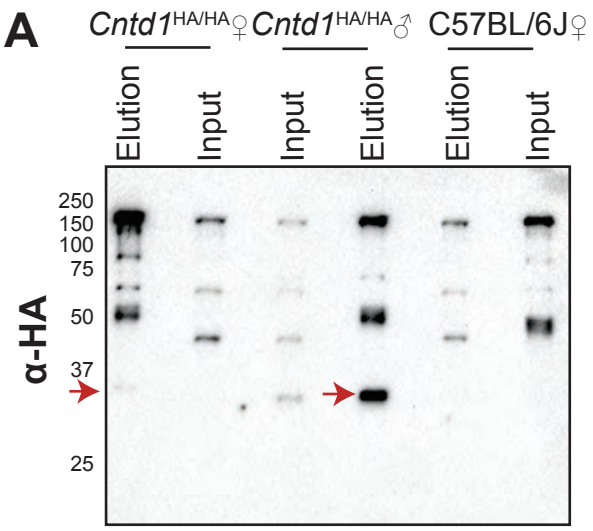
A
Cntd1HA/HA♀
Cntd1HA/HA♂
C57BL/6J♀
Elution
Input
Input
Elution
Elution
Input
α-HA
250
150
100
75
50
37
25

Wood et al., Figure 3.

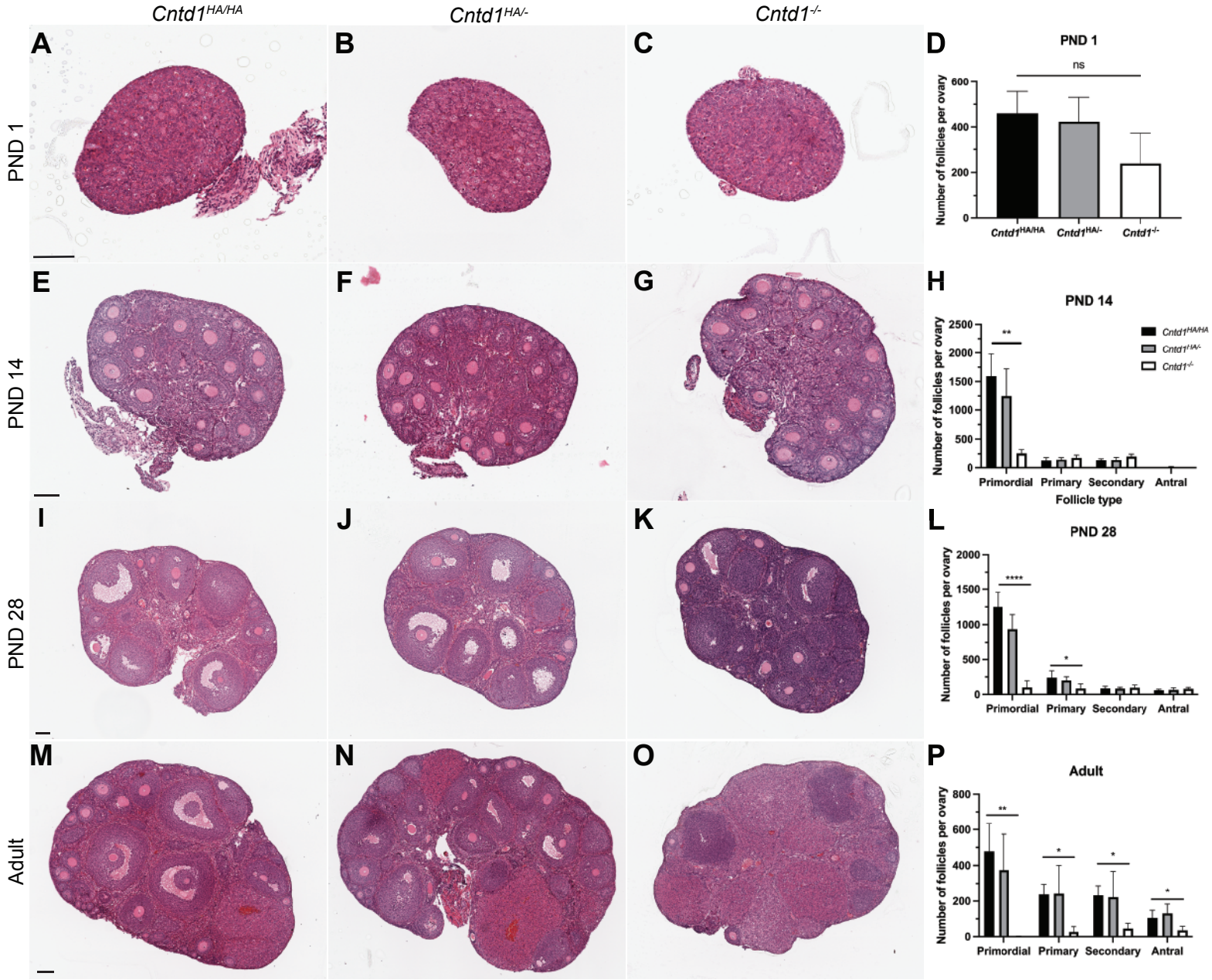

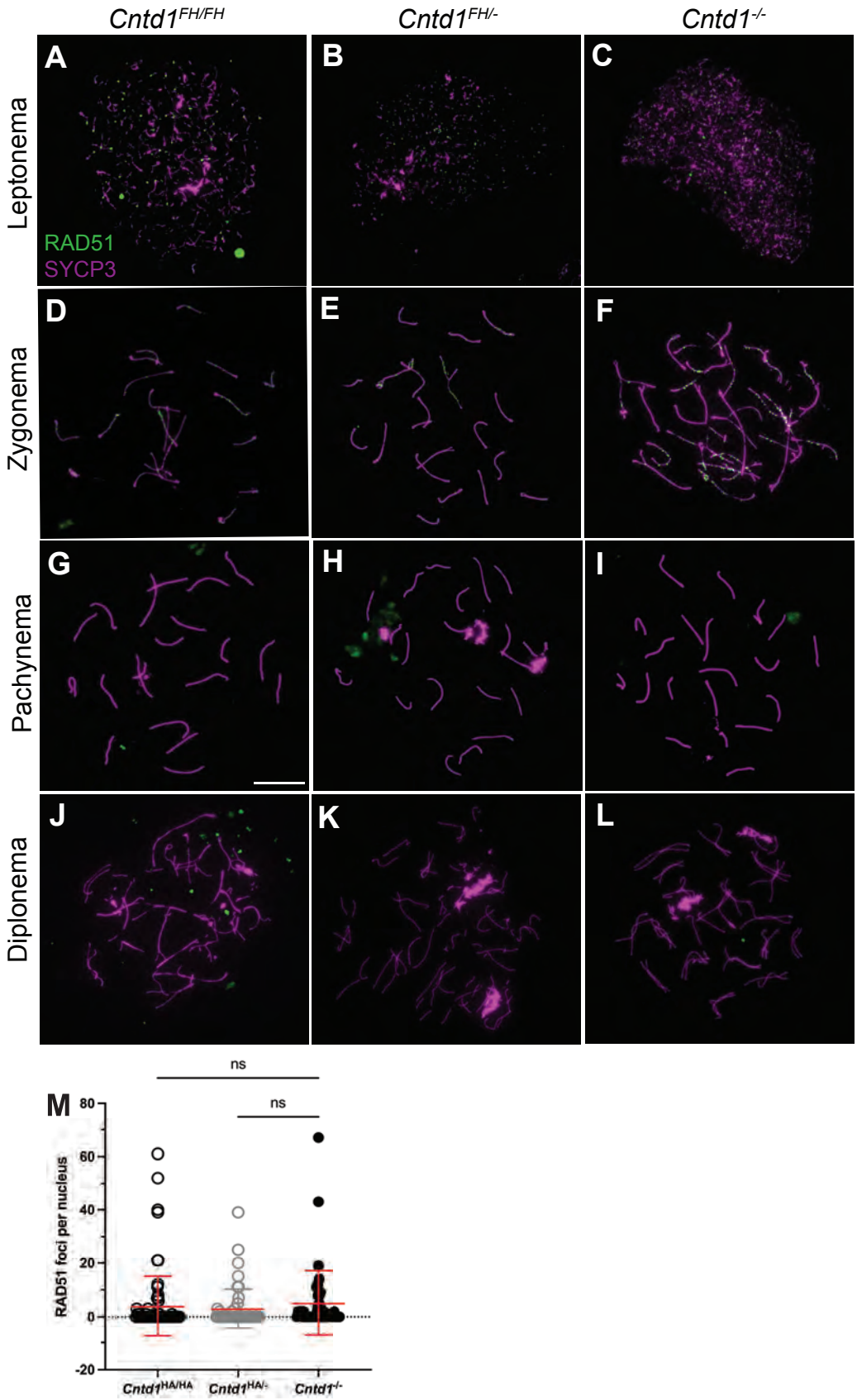
Cntd1FH/FH
Cntd1FH/-
Cntd1-/-
Leptonema
Zygonema
Pachynema
Diplonema
A
B
C
D
E
F
G
H
I
J
K
L
RAD51
SYCP3
M
ns
ns
RAD51 foci per nucleus
80
60
40
20
0
-20
Cntd1HA/HA
Cntd1HA/-
Cntd1-/-

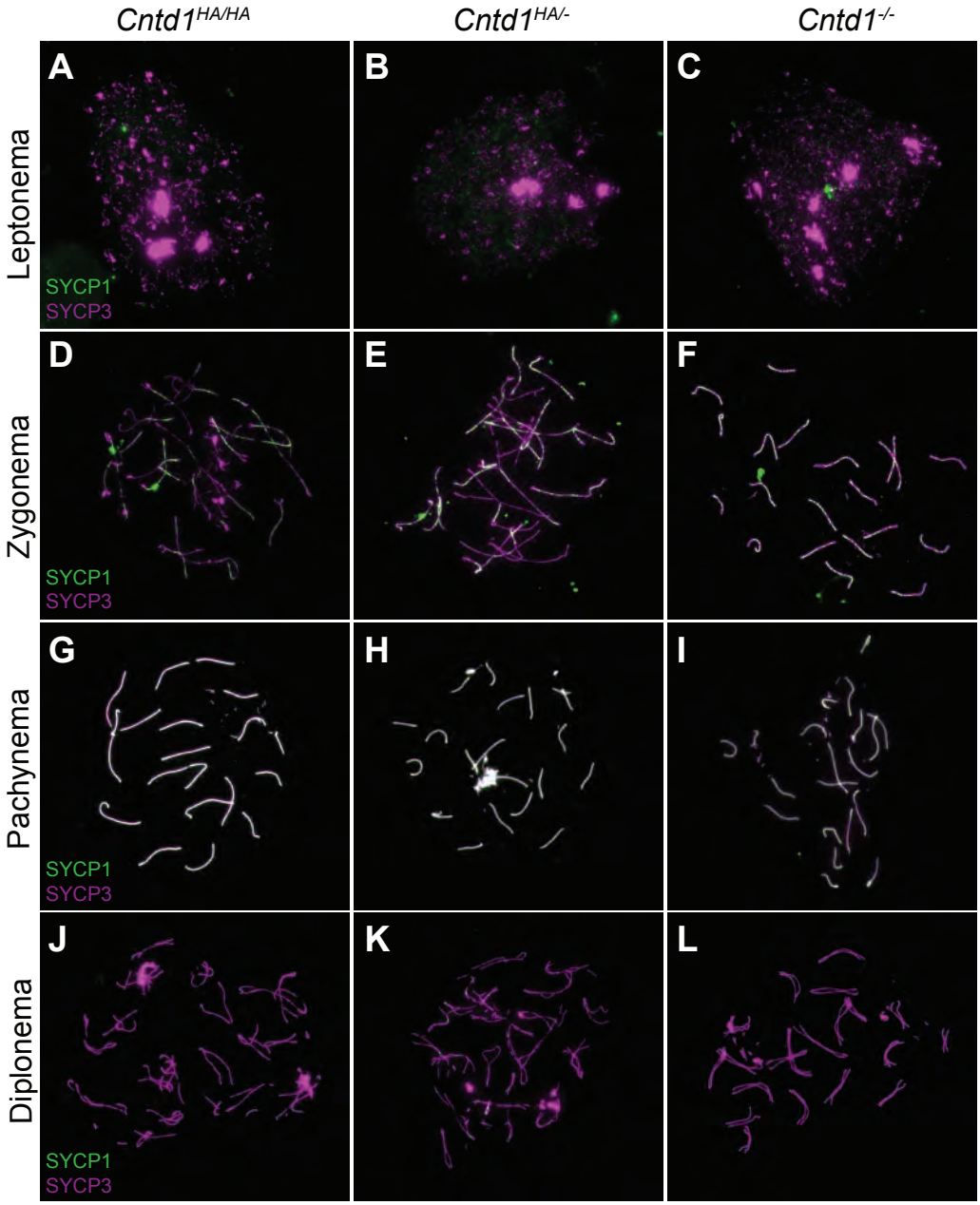
Cntd1HA/HA
Cntd1HA/-
Cntd1-/-
Leptonema
Zygonema
Pachynema
Diplonema
A
B
C
D
E
F
G
H
I
J
K
L
SYCP1
SYCP3
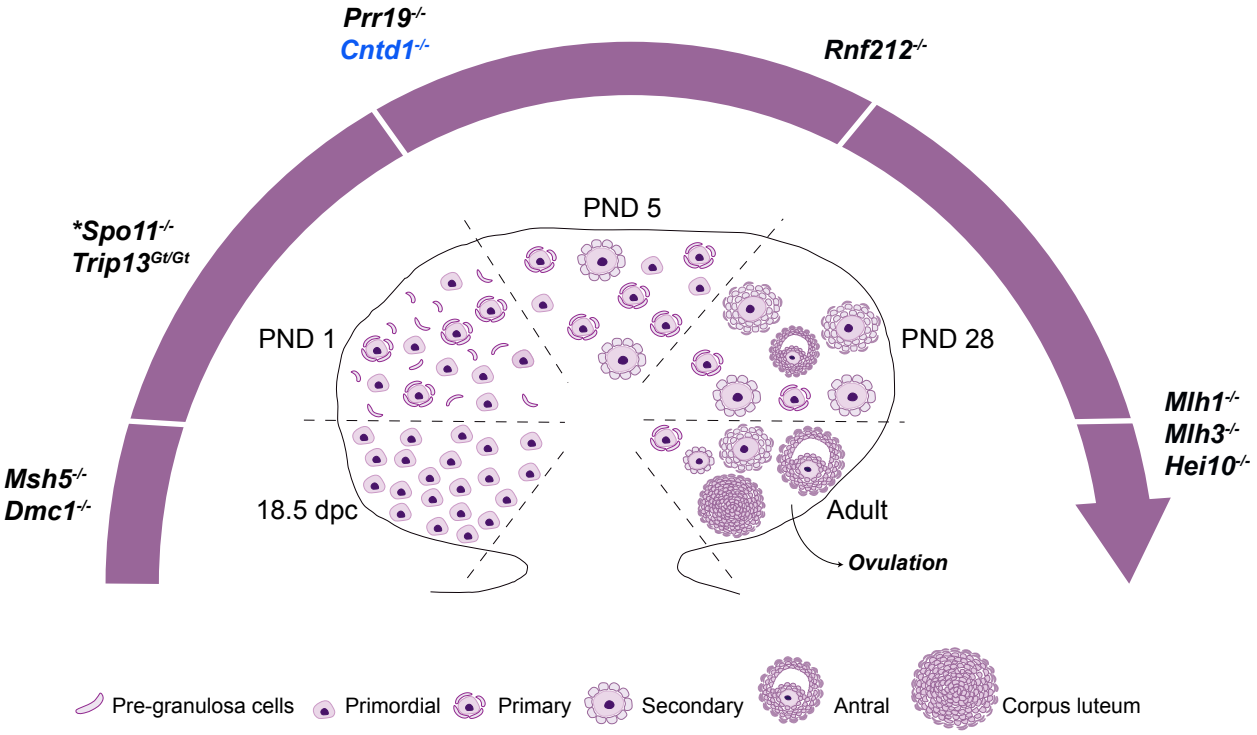
Wood et al., Figure 6.